EBioMedicine 51 (2020) 102526

Contents lists available at ScienceDirect

EBioMedicine

journal homepage: www.elsevier.com/locate/ebiom

Research paper

Ontological analyses reveal clinically-significant clear cell renal cell carcinoma subtypes with convergent evolutionary trajectories into an aggressive type

Qi Cai[a,1], Alana Christie[f,1], Satwik Rajaram[b], Qinbo Zhou[b], Ellen Araj[a], Suneetha Chintalapati[a], Jeffrey Cadeddu[c,f], Vitaly Margulis[c,f,g], Ivan Pedrosa[c,d,f], Dinesh Rakheja[a,f], Renee M. McKay[f], James Brugarolas[e,f,*], Payal Kapur[a,c,f,*]

[a] Department of Pathology, University of Texas Southwestern Medical Center, Dallas, TX 75390, United States
[b] Department of Bioinformatics, University of Texas Southwestern Medical Center, Dallas, TX 75390, United States
[c] Department of Urology, University of Texas Southwestern Medical Center, Dallas, TX 75390, United States
[d] Department of Radiology, University of Texas Southwestern Medical Center, Dallas, TX 75390, United States
[e] Department of Internal Medicine, Hematology-Oncology Division, University of Texas Southwestern Medical Center, Dallas, TX 75390, United States
[f] Kidney Cancer Program, Simmons Comprehensive Cancer Center, University of Texas Southwestern Medical Center, Dallas, TX 75390, United States
[g] Institute for Urology and Reproductive Health, Sechenov University, Moscow, Russia

ARTICLE INFO

Article history:
Received 24 August 2019
Revised 22 October 2019
Accepted 29 October 2019
Available online 16 December 2019

Keywords:
ccRCC
Morphologic heterogeneity
Prognosis
Tumor evolution
Angiogenesis inhibitors
TKIs
Immune checkpoint inhibitors

ABSTRACT

Background: Clear cell renal cell carcinoma (ccRCC) is a particularly challenging tumor type because of its extensive phenotypic variability as well as intra-tumoral heterogeneity (ITH). Clinically, this complexity has been reduced to a handful of pathological variables such as stage, grade and necrosis, but these variables fail to capture the breadth of the disease. How different phenotypes affect patient prognosis and influence therapeutic response is poorly understood. Extensive ITH illustrates remarkable plasticity, providing a framework to study tumor evolution. While multiregional genomic analyses have shown evolution from an ancient clone that acquires metastatic competency over time, these studies have been conducted agnostic to morphological cues and phenotypic plasticity.

Methods: We established a systematic ontology of ccRCC phenotypic variability by developing a multiscale framework along three fundamental axes: tumor architecture, cytology and the microenvironment. We defined 33 parameters, which we comprehensively evaluated in 549 consecutive ccRCCs retrospectively. We systematically evaluated the impact of each parameter on patient outcomes, and assessed their contribution through multivariate analyses. We measured therapeutic impact in the context of anti-angiogenic therapies. We applied dimensionality reduction by t-distributed stochastic neighbor embedding (t-SNE) algorithms to tumor architectures for the study of tumor evolution superimposing tumor size and grade vectors. Evolutionary models were refined through empirical analyses of directed evolution of tumor intravascular extensions, and metastatic competency (as determined by tumor reconstitution in a heterologous host).

Findings: We discovered several novel ccRCC phenotypes, developed an integrated taxonomy, and identified features that improve current prognostic models. We identified a subset of ccRCCs refractory to anti-angiogenic therapies. We developed a model of tumor evolution, which revealed converging evolutionary trajectories into an aggressive type.

Interpretation: This work serves as a paradigm for deconvoluting tumor complexity and illustrates how morphological analyses can improve our understanding of ccRCC pleiotropy. We identified several subtypes associated with aggressive biology, and differential response to targeted therapies. By analyzing patterns of spatial and temporal co-occurrence, intravascular tumor extensions and metastatic competency, we were able to identify distinct trajectories of convergent phenotypic evolution.

* Corresponding authors at: Kidney Cancer Program, Simmons Comprehensive Cancer Center, University of Texas Southwestern Medical Center, Dallas, TX 75390, United States.
E-mail addresses: james.brugarolas@utsouthwestern.edu (J. Brugarolas), payal.kapur@utsouthwestern.edu (P. Kapur).
[1] Qi Cai, and Alana Christie have contributed equally to this study.

https://doi.org/10.1016/j.ebiom.2019.10.052

Research in context

Evidence before this study

Clear cell renal cell carcinoma (ccRCC) is remarkable for its heterogeneity, both intratumorally and across patients. This heterogeneity poses challenges in predicting oncologic behavior, but can be leveraged to study tumor evolution. In a series of elegant reports, the TRACERx Renal consortium showed that during ccRCC development, spatial and temporal subclones evolve and coexist in different areas of the tumor all arising from a shared ancestor. What these exciting reports failed to consider, however, is ccRCC's phenotypic plasticity. Moreover, the utility of multiregional sequencing for clinical decision making remains to be determined and is limited by cost, turn-around times, and technical challenge.

Added value of this study

We provide a systematic and comprehensive ontology that captures the breadth of ccRCC phenotypes and develop evolutionary models. We: (i) identified nine dominant architectural patterns and twenty-four cytological and microenvironment features that frequently occur in ccRCC; (ii) defined subtypes associated with aggressive biology, worse outcomes in patients, and drug resistance; and (iii) established distinct trajectories of phenotypic evolution. We developed evolutionary models that incorporate directionality provided by intravascular tumor extensions as well as surrogates of metastatic competency.

Implications of all the available evidence

This is the first study to comprehensively evaluate the spectrum of phenotypic heterogeneity in ccRCC and assess its impact on clinical behavior. We report novel trajectories of tumor evolution in intravascular tumor extensions and towards the acquisition of metastatic potential. This work provides a detailed atlas of ccRCC phenotypes that can be used as a guide to improve clinical management.

1. Introduction

Clear cell renal cell carcinoma (ccRCC), the most common renal cell carcinoma (RCC) subtype, exhibits variable clinical behavior. At one end of the spectrum are small renal masses ($\leq$4 cm in size), for which active surveillance is increasingly recommended [1,2]. At the other end of the spectrum is metastatic ccRCC, which can range from limited oligometastases, which can be managed with focal therapies [3], to widespread disease requiring systemic therapies. Up to one-third of patients with apparently localized ccRCC relapse after surgery with curative intent, and another third later present with regional or distant metastasis [4]. ccRCC can colonize a wide range of distant sites, some of which seem to confer a differential prognosis. For example, hepatic metastases have a worse prognosis than pancreatic metastases [5,6].

ccRCC is recognized as one of the most diverse tumors histologically. This diversity is observed not only across patients, but also within tumors. Histopathologic intratumoral heterogeneity (ITH) has been appreciated for decades [7–9]. This daunting complexity has been reduced to a small subset of clinical variables including stage, grade and necrosis, which are unlikely to capture the breadth of the disease. Tumor grade is based largely on nucleolar size. Pathological analyses also incorporate isolated elements such sarcomatoid and rhabdoid morphologies. Nevertheless, morphological analyses have remained the gold standard for cancer diagnosis and prognosis, which is a testament to the power of morphology.

At the molecular level, ccRCC has been shown to harbor remarkable ITH [10–14]. Multiple studies have examined ccRCC ITH using next-generation sequencing tools and evaluated the clinical significance [13–15]. The TRACERx Renal study is the largest multiregional profiling effort to date, evaluating data from 1206 regions across 106 primary tumors in 101 RCC patients [14]. From these data, it has been proposed that during ccRCC development, spatial and temporal subclones evolve and coexist in different areas of the tumor. Based on these data, ccRCC has been genomically grouped into seven evolutionary subtypes [14] that exhibit different clinical outcomes. Unexpectedly, this diversity emerges from a relatively small number of core tumor suppressor genes converging on a particular region of the genome on chromosome 3p [12,16].

While extensive studies have been performed to evaluate genetic heterogeneity and tumor evolution, little is known about phenotypic evolution. As a clonal disease, the extensive phenotypic heterogeneity of ccRCC reports on a natural evolutionary process and shows remarkable plasticity. This morphological heterogeneity is likely an expression of genomic heterogeneity. In fact, our previous studies documented that subclonal loss of driver genes in ccRCC, such as *BAP1* and *PBRM1*, resulted in different morphologic features in the corresponding tumor areas [12,17–19].

The implications of ccRCC phenotypes remains largely unaddressed. However, this is likely to hold important cues for patients, and several treatments approved for ccRCC are linked to phenotype. For instance, the largest class of approved drugs targets angiogenesis, which is highly variable across tumors. In addition, recently approved checkpoint inhibitors depend upon a primed immune system and their activity is likely related to the presence of an immune infiltrate, which is also quite diverse across and within tumors.

Here, we aimed to dissect ccRCC morphologic heterogeneity, to identify evolutionary patterns of tumor phenotypes and to evaluate their association with clinical outcomes. The goals of the study were: (1) to produce a systematic and comprehensive ontology that captured the breadth of ccRCC phenotypes; (2) explore their clinical implications; and (3) develop an evolutionary model of tissue phenotypes. To this end, we developed a multiscale framework to dissect ccRCC heterogeneity according to three fundamental axes: tumor cytology, architecture and the microenvironment. We systematically applied this approach to 549 tumors with complete clinical history and assessed its significance, in terms of prognosis and response to anti-angiogenesis agents. In addition, we developed an evolutionary model, which we validated in the context of directional intravascular invasion and metastatic competency, as established by recapitulation of the tumorigenesis process in a heterologous host.

2. Materials and methods

2.1. Study population

All neoadjuvant therapy-naïve nephrectomy samples diagnosed as ccRCC at our institution between 2006 and 2015 with available H&E-stained diagnostic slides were retrieved. The study did not include consultation cases or biopsy specimens. We excluded patients with follow-up $<$1.5 years unless the patients were known to have died. Confirmation of the ccRCC diagnosis was performed for each case by a genitourinary (GU) pathologist (P.K.). The tumors were classified as ccRCC based on the 2016 WHO classification [20]. Tumors diagnosed as ccRCC prior to 2010 but with the morphology of recently described entities, such as clear cell papillary RCC, TCEB1 mutation-associated RCC, or MiTF translocation

RCC, were excluded from this study [20]. Diagnoses were aided, where required (such as in high-grade tumors lacking the classic morphology), by immunohistochemistry, including analyses for diffuse membranous expression of carbonic anhydrase-IX. All cases were adequately sampled according to published recommendations [21] (minimal 1 block/cm of tumor diameter, sampling of all visually disparate areas, and <3 cm tumors completely submitted). Out of a total of 1058 ccRCC cases, 549 met the above selection criteria and were comprehensively reviewed. The study was approved by the UT Southwestern Medical Center (UTSW) Institutional Review Board (IRB) and conducted according to the Health Insurance Portability and Accountability Act (HIPAA) guidelines.

2.2. Data collection

Comprehensive clinical and pathology data were collected retrospectively through the Kidney Cancer Explorer database (KCE), an i2b2-based institutional RCC database that integrates clinicopathologic data from electronic medical records (sponsored by the UTSW Kidney Cancer NIH SPORE grant, the Lyda Hill Department of Bioinformatics and the Bioinformatics Core Facility). The originally reported grade was based on the year the diagnosis was recorded using Fuhrman nuclear grading or the nucleolar grading system. Subsequently, a centrally reviewed grade based on the nucleolar grading system was generated and used for all statistical analyses. Tumor grade was adjusted in 17 of the 549 ccRCCs using the International Society of Urological Pathology (ISUP) criteria. Because all cases were resected prior to 2016, the 2010 American Joint Committee on Cancer (AJCC) TNM classification was used for pathologic staging. Parenthetically, only one case would have been upstaged from pT1b to pT3a if using the 2018 AJCC classification.

2.3. Study outcomes

The end-points evaluated were disease-free survival (DFS), which was calculated from the date of surgery to the date of first metastasis/recurrence or death; and overall survival (OS), which was calculated from the date of surgery to the date of death from any cause. Metastatic RCC was defined as the presence of a distant lymph node and/or organ metastasis. If available, the date of biopsy was used or, if not available, the date of initiation of therapy [systemic therapy, surgery, or radiation]. Only when neither was available, was date of imaging confirming distant metastasis/recurrence used. Survival of patients who were lost to follow-up was censored at the date of last contact. Outcome data were retrieved from the database on May 20, 2017. Time to next treatment was recorded for patients with metastases who were treated with a vascular endothelial growth factor/receptor inhibitor (VEGF/R-I) therapy in the frontline.

2.4. Deconvoluting ccRCC phenotypes

To comprehensively capture all the different patterns present in ccRCC, three different aspects of the tumor were assessed: (1) spatial architecture, (2) cytologic features, and (3) the tumor microenvironment (TME). Tumor samples were analyzed under a Nikon Eclipse E100-LED multihead microscope (Nikon Instruments Inc.), and the entire spectrum of morphologic features visualized in the entire case (not just the high-grade areas) was tabulated. The grading rendered in the pathology report for each case was confirmed. The estimated percentage (minimum of 5% was required) of each architectural pattern and the presence or absence of the cytologic and TME characteristics (even when focal) were tabulated for each tumor manually by 2 investigators who were blinded to the patient diagnosis and clinical information.

2.5. Minimizing interobserver variability

In order to minimize interobserver variability, the morphologic features were evaluated in two batches. The first 100 cases were reviewed together by two pathologists in the current study (a GU pathology fellow in training (Q.C.) and a senior GU pathologist (P.K.) with >15 years of experience). The two pathologists working together generated: (a) an atlas of each pattern to serve as a reference, and (b) a table enumerating all the features in each of the 100 cases. The remaining cases were independently analyzed by the GU pathology fellow (Q.C.). Cases with multiple architectures (>2 different patterns), all grade 3 and 4 tumors, and any tumors with uncertainty were re-evaluated by both pathologists to confirm the results. The concordance rate for the different patterns was 95% between the two pathologists (Q.C. & P.K.). To assess interobserver reproducibility, a third pathologist (S.C) independently reviewed 40 randomly selected cases after being provided the atlas of the architectural patterns. The concordance rate between the 3rd independent pathologist and the prior assessment was 95% (38/40 cases were concordant)

2.6. Immunohistochemistry

Immunohistochemical analysis for CD31 as described previously [22] was performed on representative tumors to highlight the vascular network.

2.7. Statistical analysis

Data were descriptively summarized using frequencies and percentages for categorical variables and means, medians, standard deviations, and ranges for continuous variables. Chi-square tests were used to test for associations between categorical features and clinicopathologic parameters, while Student's *t*-test (for two groups) or ANOVA (for three or more groups) were used to test for differences in continuous measures among the clinicopathologic features. A swimmer's plot was used to visualize both time on VEGF/R-I therapy and predominant architecture. Kaplan-Meier curves were generated to visualize survival distributions, and the log-rank test was used to analyze differences in survival. Heatmaps were generated based on conditional probabilities of two patterns occurring together, as well as for the enrichment of patterns present together. All p values were 2-sided, and p values <0.05 were considered statistically significant. A correction for multiple testing was made using an FDR adjustment on the Chi-square p-values. Statistical analyses were conducted using SAS 9.4 (SAS Institute Inc., Cary, NC).

2.8. Multivariate Cox regression model

Multivariate Cox regression models for disease free survival (DFS) were built using backwards selection with exclusion of factors with $p \geq 0.05$. All architecture, cytology, and microenvironment parameters that showed statistical significance in the univariate analysis were included. Models were built with and without nucleolar grade. The nomogram based on the multivariate model including nucleolar grade was built using the rms package in R [23].

2.9. t-distributed stochastic neighbor embedding (t-SNE)

Each primary sample was characterized in terms of the nine-dimensional architectural composition vector, viz., the percentage of the area occupied by each of the 9 architectures. Global patterns of similarity between the samples were visualized in 2-dimensions using t-SNE [24]. Briefly, t-SNE attempts to represent each nine-dimensional profile based on a 2-D point such that points that

are neighbors in the nine-dimensional space (quantified by the Euclidean distance) are also neighbors in their 2D representations. t-SNE was implemented using the manifold.TSNEfunction in the scikit-learn python package with default parameters (perplexity = 30). Repeated embeddings (differing in random initial conditions) were found to produce qualitatively similar results.

2.10. Patient-derived xenograft model evaluation

To assess metastasis competency of particular regions in the tumor, we leveraged the Kidney Cancer Program patient-derived xenograft (PDX) platform. Among the 549 patients included in this study, 174 tumor fragments (1–3 mm in diameter) from 149 patient tumors were implanted orthotopically (under the renal capsule) in nonobese diabetic/severe combined immunodeficient (NOD/SCID) mice (2–5 mice per sample) and evaluated for their ability to form tumors. Architectural patterns were determined by H&E analyses of the immediately flanking sections as described previously [25,26]. Out of the 149 patients, 134 patients had one sample implanted and 15 had multiple (7 patients with 2; 6 patients with 3; and 2 patients with 4 samples). To assess the ability of the tumor sample to grow in a heterologous host (which we regard as metastasis competency), we scored for stable engraftment – histologically validated tumors passaged at least twice in mice. Rates of stable engraftment were assessed for each architectural pattern. Odds ratios were used to compare engraftment rates. To account for the dependence in the data where patients had multiple samples implanted in mice, a GEE model using a logit link and binary distribution was used to model the odds ratio for engraftment in aggressive patterns (alveolar, solid sheet, papillary/pseudopapillary, thick trabecular/insular) compared to indolent patterns (microcystic, tubular/acinar, compact small nests, large nests). The covariance structure was treated as compound symmetric.

3. Results

3.1. Baseline clinical characteristics of the study population

A total of 549 consecutive patients with ccRCC were included in this study. Patient demographics, as well as the distribution of tumor grade and stage, is shown in Supplemental Table S1, and were representative of most large referral centers [17,27]. The mean age at diagnosis was 59.8 years (range 24–86), and there were more males than females (~3:2 ratio). Nearly 50% of the tumors were of high grade (3 or 4), and one third of high stage (pT3 or pT4). Among the 117 (21.3%) patients with metastatic disease, 45 (8.2%) had metastases at the time of nephrectomy (M1). The mean duration of follow-up was 4.0 years (median 3.5; range 1 day [due to the inclusion of cases with post-surgical death]−11.3 years).

3.2. Nine distinct architectural patterns frequently occur in ccRCC

We established three axes along which to characterize tissue phenotypes: tumor cytology, architecture and the microenvironment. Based on these axes, we defined 33 variables and assessed their frequency across the entire tumor cohort (Supplemental Table S2). Although some of our observed patterns have been reported previously [9], several additional patterns were identified. Fig. 1 shows representative images of the distinct features analyzed to make our categories functionally implementable in a clinical setting.

The distinct architectural patterns that we observed included compact small nests (hereinafter in text called compact nests), large nests, thick trabecular/insular (hereinafter in text called insular), solid sheet (hereinafter in text called solid), microcystic, tubular/acinar (hereinafter in text called tubular), bleeding follicles, alveolar, and papillary/pseudopapillary (hereinafter in text called papillary) (Fig. 1a). Rare patterns, such as sieve-like, gland-like, and cribriform were observed in <10 cases each and were grouped with the solid sheet category based on a shared spaced-out vascular network (Supplemental Figure S1). We considered subdividing the large nest category to account for tumors with dilated vascular channels, but did not do so as they did not exhibit clinical or prognostic differences (see below).

3.3. Twenty-four unique cytologic and TME patterns frequently occur in ccRCC

We next evaluated the spectrum and frequencies of unique cytologic (Fig. 1b) and tumor microenvironment (TME) features (Fig. 1c), which are also listed in Supplemental Table S2. These features included cytologic features resembling previously described entities, such as hereditary leiomyomatosis and RCC-like (HLRCC-like), clear cell papillary RCC-like (ccPRCC-like), chromophobe RCC-like (ChRCC-like). In addition, we evaluated cytoplasmic features, such as cytoplasm abundance (translocation-RCC (tRCC)-like, hereinafter in text called tRCC), and the presence of cytoplasmic hyaline globules. We also noted the presence of rhabdoid or sarcomatoid differentiation, as well as tumor giant cells (both degenerate appearing and syncytial giant cells).

For TME features, we evaluated the tumor border, stroma, and inflammatory infiltrate. We assessed for the presence of necrosis, a central scar, the type of intratumoral stroma, as well as the location and type of inflammation. We evaluated for infiltration into the renal parenchyma (with either nodular, sheet-like and single cell patterns) and the presence of non-sinus lymphovascular invasion (LVI).

The frequencies of previously described features, such as sarcomatoid or rhabdoid morphology, and tumor necrosis, were 4.2%, 4.9%, and 16.8%, respectively. These frequencies are similar to those reported in previous studies [28]. One feature that is underappreciated and underreported in the literature but that we observed at a high frequency (65.6%) was the presence of central scarring, a feature suggestive of regression changes (Supplemental Figure S2). Tumors as small as 1.5 cm showed this feature, which ranged from an edematous vascularized stroma lacking tumor cells to a more collagenized scar-like central area. In summary, we identified twenty-four unique cytologic and TME features in ccRCC.

3.4. Widespread intratumoral architectural heterogeneity is seen in ccRCC

We observed widespread ITH in the tissue architecture. Most tumors showed multiple different patterns per tumor (476/549, 86.7%). An average of 3 patterns per tumor (std. dev., 1.4; range, 1–7 patterns/tumor) was observed. 229 (41.7%) tumors showed prominent ITH with >3 patterns.

Among the nine distinct architectural patterns that occurred frequently in ccRCC (Supplemental Table S2 and Fig. 1a), compact nests and large nests were the most common (74.3% and 57.7%, respectively). Compact nests and large nests represent the most classic patterns associated with ccRCC [8]. We also found a statistically significant association between the presence of a larger number of patterns and higher nucleolar grade, higher pT stage category, TNM stage, and the presence of metastasis (all $p < 0.0001$; Supplemental Table S3).

In addition, widespread variability in tumor microenvironment and cytologic heterogeneity was also observed. Different cytologic features were observed in different regions of the tumor, sometimes within similar architectural patterns; and similar cytologic features were sometimes observed within the same region of the tumor but with different architectural patterns.

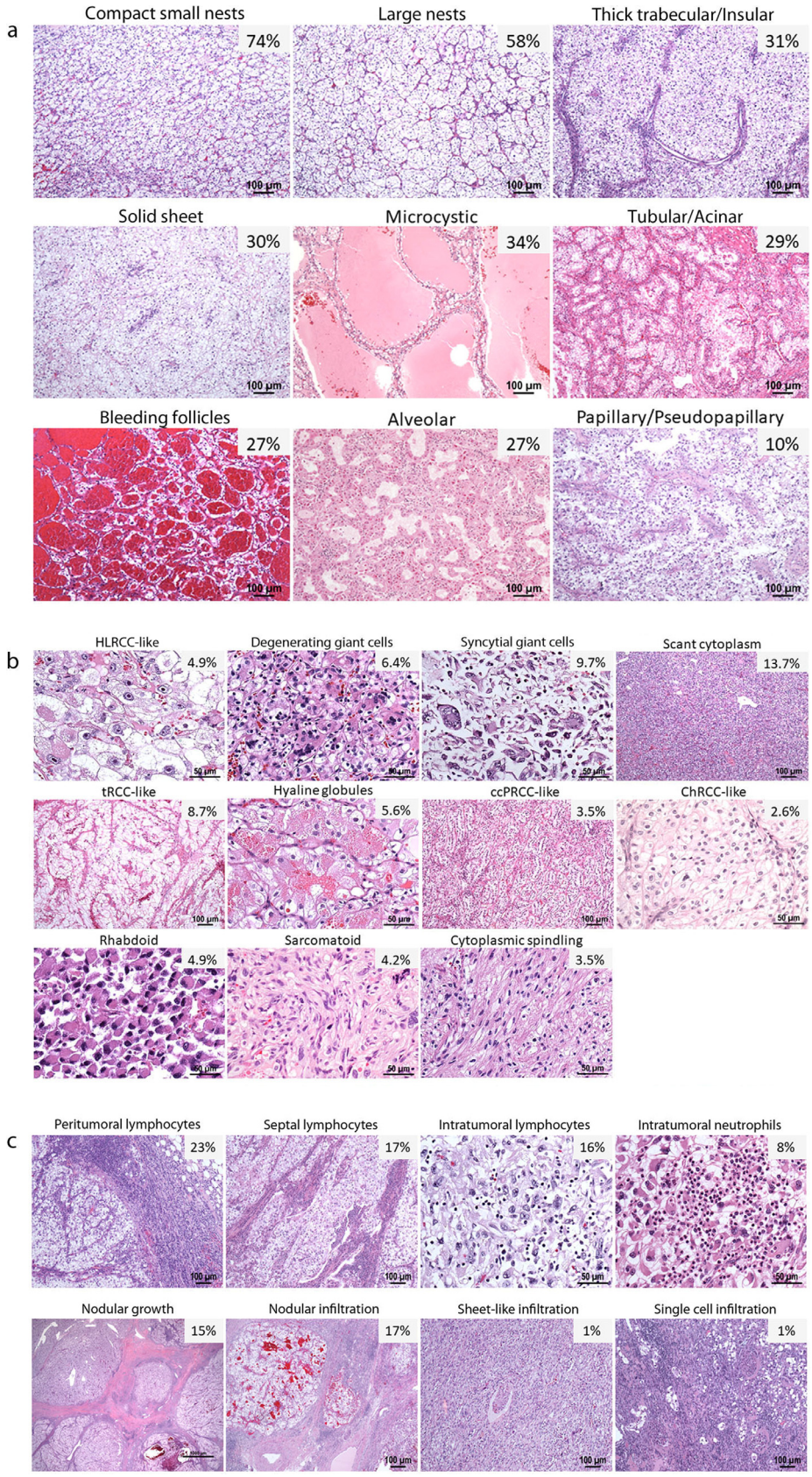

Fig. 1. Spectrum of common phenotypic subtypes in ccRCC. Representative H&E-stained images of ccRCCs showing the following subtypes and their frequencies in our cohort ($n = 549$). **(a) Architectural features:** compact small nests, large nests, thick trabecular/insular, solid sheet, microcystic, tubular/acinar, bleeding follicles, alveolar and papillary/pseudopapillary. **(b) Cytologic features**: hereditary leiomyomatosis and RCC (HLRCC)-like, degenerating giant cells, syncytial giant cells, tumor cells with scant cytoplasm, tumors with abundant cytoplasm/translocation RCC (tRCC)-like, cytoplasmic hyaline globules, clear cell papillary RCC (ccPRCC)-like, chromophobe-RCC (ChRCC)-like, rhabdoid, sarcomatoid, and cytoplasmic spindling. **(c) Tumor microenvironment (TME):** peritumoral, septal, and intratumoral lymphoplasmacytic infiltrates, intratumoral neutrophilic infiltrate, nodular growth, tumor infiltration into the renal parenchyma (nodular, sheet-like or single cell pattern).

3.5. Specific architectural patterns correlate with prognostic variables

To explore the clinical significance of the architectural patterns identified, we performed a chi-square test to determine how they related to ccRCC prognostic variables. We evaluated correlations with nucleolar grade, pathological T stage, overall TNM stage (at diagnosis), and development of metastases (Fig. 2a). One challenge we faced in correlating patterns with prognostic variables was ITH. Most tumors comprised of multiple different patterns and a given pattern may account for only a fraction of the entire tumor. Despite this challenge, we found that specific patterns correlated with known prognostic variables assigned to the entire tumor. Overall, tumors containing microcysts, bleeding follicles and/or compact nests had low overall nucleolar grade, organ-confined disease (pT1-2), low TNM stage, and infrequently developed metastases (all Chi-square FDR-$q < 0.05$; Fig. 2a). By contrast, tumors containing alveolar, papillary, insular, and/or solid components were typically of high nucleolar grade, high TNM stage, and frequently developed metastases (all Chi-square FDR-$q < 0.05$; Fig. 2a). These data imply that the presence of a subset of architectural patterns, irrespective of the amount or presence of other patterns, is informative of tumor aggressiveness.

3.6. Distinct cytologic and TME features are associated with advanced TNM stage and increased risk of metastasis

We next extended the analysis to include cytologic and TME features (Fig. 2b,c). In addition to sarcomatoid and rhabdoid features (which are by definition grade 4), the presence of the following features (even though focal) were associated with a high overall nucleolar grade (grade 3–4): HLRCC-like, giant cells, tRCC-like, hyaline globules, ChRCC-like, cytoplasmic spindling, a nodular growth pattern, abundant lymphoplasmacytic or neutrophilic infiltrate, tumor necrosis, LVI, and infiltration into the renal parenchyma. All of the above cytologic patterns were also associated with a high pathological T stage (pT3-4), high TNM stage and an increased risk of metastasis (all Chi-square FDR-$q < 0.01$; Fig. 2b,c).

Currently, College of American Pathologists (CAP) primary tumor (pT) staging guidelines are based on tumor size (when limited to the kidney) or tumor invasion specifically into (i) the perinephric tissues, (ii) renal sinus, or (iii) major vein/its segmental branches (pT3) [21]. Infiltration into the renal parenchyma is not considered. However, we found that infiltration into the renal parenchyma is not uncommon (116 tumors) and that it is not always associated with infiltration into perinephric tissue, the renal sinus or major vessels. Specifically, we identified 32 tumors that infiltrated into the parenchyma, but not elsewhere (in spite of extensive renal sinus sampling). Based on current staging criteria, these tumors would be staged as pT2 or pT1. However, 11 out of the 32 patients developed metastasis. This rate of metastasis (~30%) is in contrast to that expected for pT2 or pT1 tumors (<7%) and similar to pT3 tumors [4]. These data suggest that intraparenchymal invasion may be prognostic even if found in isolation.

3.7. Phenotypic patterns correlate with survival in patients with localized and advanced ccRCC

Given the association between prognostic variables and the presence of particular architectural, cytologic, and TME features, we next evaluated the association between the presence of these morphologic patterns and disease-free survival (DFS) and overall survival (OS) in the entire cohort (Fig. 3, Supplemental Figure S3, S4a-b). As previously reported [28,29], our log-rank analysis found that patients with sarcomatoid and rhabdoid morphologies as well as tumor necrosis had significantly worse DFS and OS compared to patients without these features (all log-rank $p < 0.0001$; Fig. 3b and Supplemental Figure S4b).

A univariate analysis showed that patients with aggressive architectures (i.e., alveolar, papillary, insular, and solid) or cytologic and TME features (i.e., tumor giant cells, ChRCC-like, HLRCC-like, tRCC-like, hyaline globules, intratumoral lymphoplasmacytic and neutrophilic infiltrate, nodular growth, LVI, and tumor infiltration into the renal parenchyma) had a significantly shorter DFS than patients without these features (all log-rank $p < 0.01$; Fig. 3a,b). By contrast, patients with microcystic, tubular, or bleeding follicles and compact nests in their tumors were more likely to live longer without disease (all log-rank $p < 0.01$; Fig. 3a). Interestingly, the association between good/poor clinical behavior and the presence of insular, solid, and tubular components remained statistically significant even after stratification by grade of the entire tumor (Fig. 4a).

While more aggressive subtypes occurred at a higher frequency in tumors of higher grade/stage (Fig. 2), we wondered whether deviations from this trend could help better stratify patients within a grade. As shown in the subgroup analysis in Fig. 4b, occurrence of some of the aggressive features (insular, solid, presence of tumor giant cells, necrosis, infiltration into renal parenchyma) in low grade tumors increases the hazard ratios for DFS, while occurrence of the more indolent tubular component in high grade tumors is indicative of better outcomes. These subgroup analyses show that grade alone may underestimate the aggressiveness of some low-grade cases and overestimate that of some high-grade tumors. For example, insular suggests poor prognosis in grade 2, but loses its utility in grade 4, while tubular and large nests are non-contributory at grade 2 but are suggestive of better prognosis at grade 4. These data suggest that presence of aggressive morphologies have prognostic implications beyond current prognostic parameters and have the potential to guide clinical decision making.

The Kaplan-Meier curves for OS are largely overlapping with DFS (except for large nests or ChRCC-like, which were not significant) and are shown in Supplemental Figure S3 and S4b. Our initial analysis included patients with synchronous metastasis, who had the most advanced ccRCCs. We therefore repeated the analyses in 504 patients with localized ccRCC at presentation (M0) and found that the architectural patterns largely maintained their association with DFS (all log-rank $p < 0.05$), with the exception of compact nests, bleeding follicles and papillary (Supplemental Figure S5). Similarly, most of the cytologic and TME features also correlated with DFS and OS in localized ccRCCs (all log-rank $p < 0.05$; Supplemental Figure S6a,b). The features with the highest DFS predictive values included alveolar, insular, solid, tRCC-like, ChRCC-like, HLRCC-like, tumor giant cells (syncytial and degenerating giant cells), cytoplasmic hyaline globules, sarcomatoid, rhabdoid, LVI, tumor infiltration into the renal parenchyma, intratumoral neutrophilic infiltrate, and tumor necrosis (Supplemental Figure S6a).

In a multivariate analysis, the presence of tRCC-like, insular, intratumoral neutrophilic infiltration, renal parenchymal infiltration, tumor necrosis, ChRCC-like, and rhabdoid features remained independent unique predictors of DFS after backwards selection (Table 1A). When the nucleolar grade was considered, the presence of tubular, necrosis, renal parenchymal infiltration, and ChRCC-like remained as independent unique predictors of DFS (Table 1B). Based on these results, we generated a nomogram (Fig. 4c).

3.8. Vascularity and response to anti-angiogenic therapy

We observed a wide spectrum in vascularity across architectures. Vascularity was maximal in the compact nests, large nests, tubular, bleeding follicle, alveolar, and microcystic components. In contrast, vascularity was reduced in insular, papillary and solid

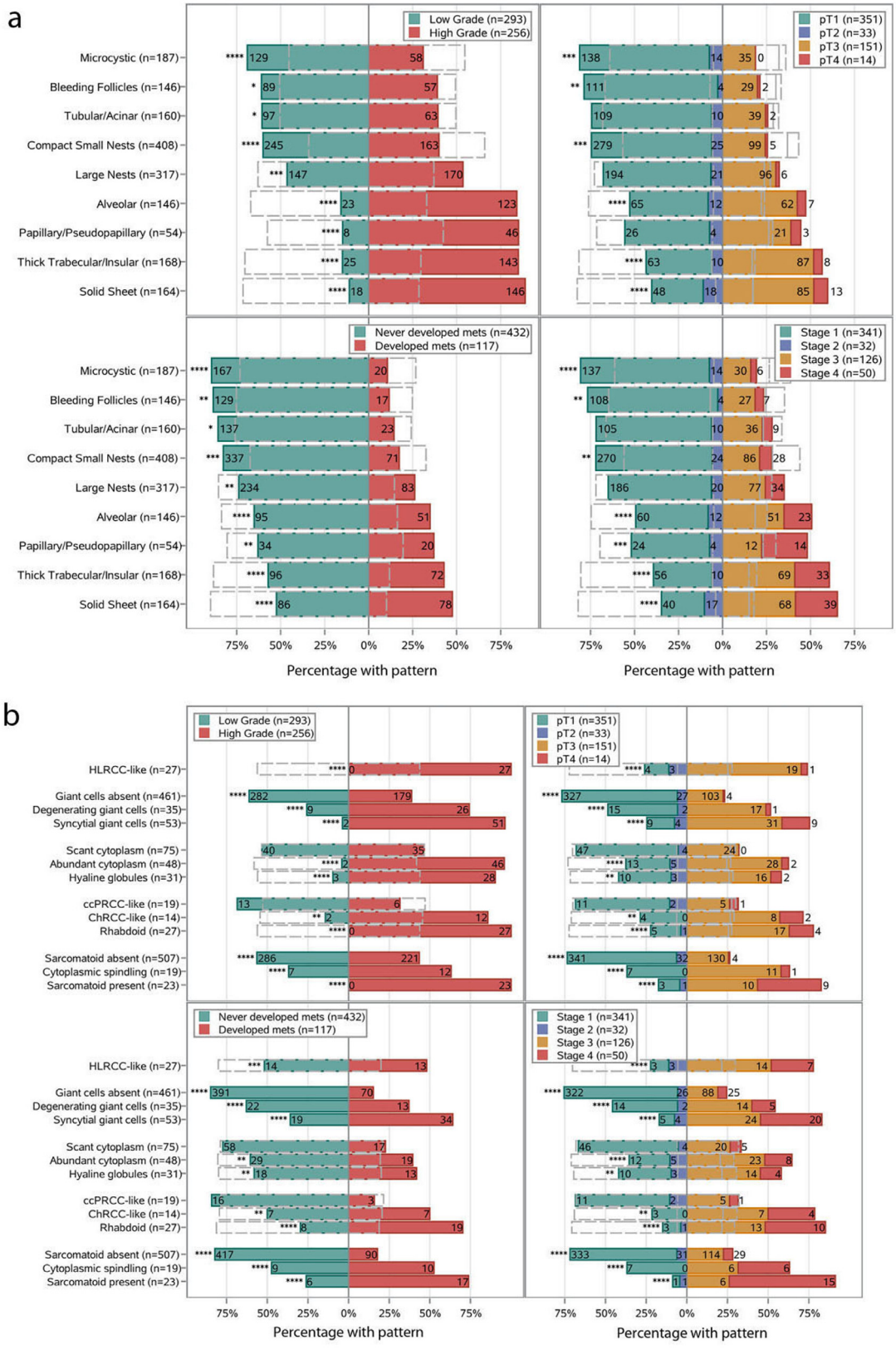

Fig. 2. Comparison of the presence of common architectural (a), cytologic (b), and TME (c) subtypes by nucleolar grade, pT substage, TNM stage at diagnosis, and metastases. Numbers and percentages represent the distribution of each variable for the presence in each subtype. The gray dashed outline represents the distribution for the absence of each subtype. The *p* value was calculated from the Chi-Square test to analyze the association between the presence/absence of a subtype with nucleolar grade, pT substage, TNM stage at diagnosis, and metastases. A correction for multiple testing was made using an FDR adjustment on the Chi-square *p*-values. FDR-*q* values are depicted as * < 0.05, ** < 0.01, *** < 0.001 and **** <0.0001.

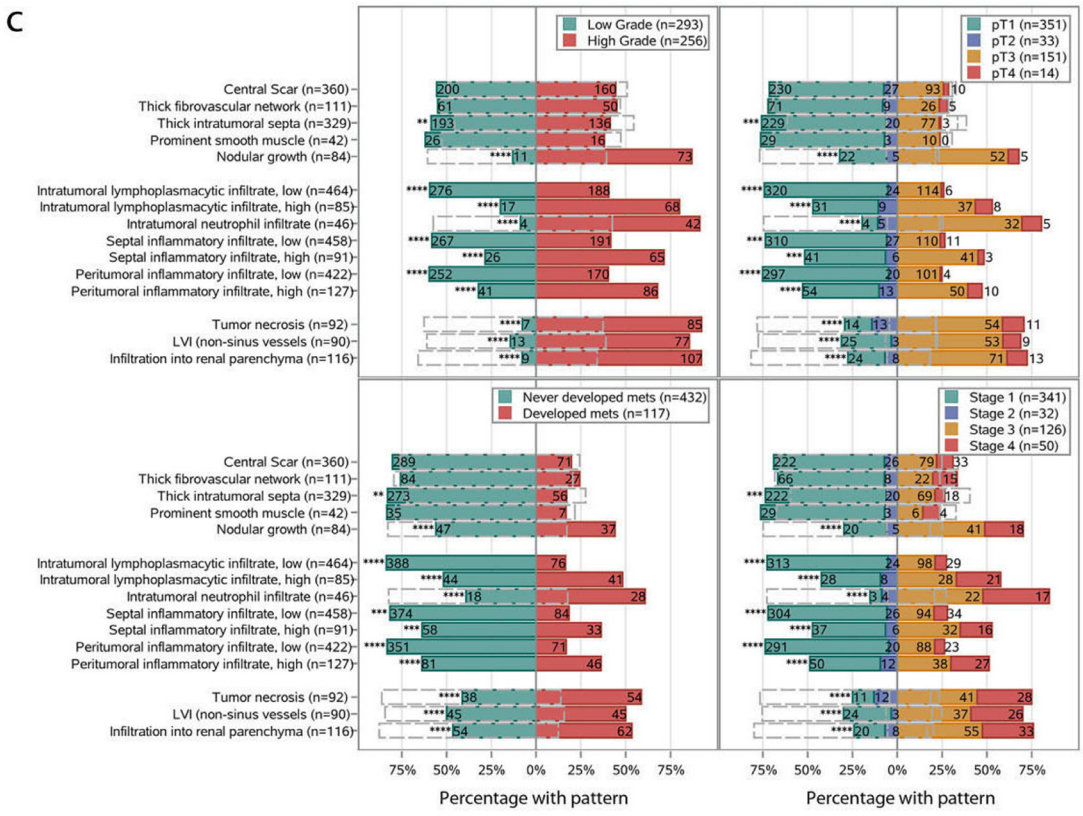

Fig. 2. Continued

Table 1A
Multivariate analysis of disease-free survival for individual variables without grade.

	Hazard Ratio (95% CI)	*p*-value
Abundant cytoplasm/tRCC-like	0.56 (0.35, 0.91)	0.0191
Presence of thick trabecular/insular pattern	1.62 (1.11, 2.36)	0.0125
Intratumoral neutrophils	1.68 (1.09, 2.61)	0.0193
Renal parenchymal infiltrative edge	2.14 (1.43, 3.21)	0.0002
Necrosis	2.15 (1.40, 3.31)	0.0005
ChRCC-like	2.61 (1.29, 5.26)	0.0075
Rhabdoid	2.77 (1.64, 4.69)	0.0001

Table 1B.
Multivariate analysis of disease-free survival for individual variables with grade.

	Hazard Ratio (95% CI)	*p*-value
Presence of a tubular/acinar pattern	0.67 (0.47, 0.96)	0.0288
Necrosis	1.74 (1.16, 2.59)	0.0070
Renal parenchymal infiltrative edge	1.80 (1.25, 2.61)	0.0017
ChRCC-like	2.54 (1.28, 5.03)	0.0078
Nucleolar Grade		
1	reference	<0.0001
2	4.86 (0.67, 35.34)	
3	10.42 (1.43, 76.09)	
4	24.59 (3.25, 185.78)	

(Supplemental Figure S7a). Given the reported association between gene expression markers of angiogenesis and improved outcomes with drugs targeting endothelial growth factor/receptor (VEGF/R) [30,31,37], we asked if there was an association between tumor patterns with vascular stroma and response to VEGF/R inhibitors (VEGF/R-I). For these analyses, we focused on patients with metastatic ccRCC who received VEGF/R-I in the frontline. We found that patients with tumors composed predominantly of a pattern characterized by reduced vascular networks had shorter time to progression (Supplemental Figure S7b). These data suggest that there may be an association of morphologic phenotypes and response to VEGF/R-I therapies.

3.9. Increased ITH correlates with increased tumor size, advanced stage, and reduced survival

Having developed this tridimensional ontology based on tumor cytology, architecture and the microenvironment, and after exploring the prognostic and predictive value of the 33 features we defined, we next focused our attention on intratumoral heterogeneity. Inasmuch as ccRCC is a clonal disease, we hypothesized that the morphological heterogeneity we observed reflected tumor plasticity and likely developed over time. Consistent with this hypothesis, we found that smaller tumors had fewer architectural patterns than larger ones, which probably evolved over a longer period of time (Fig. 5a, $p < 0.0001$). In addition, we observed that small tumors were not only more homogeneous, but also most often had compact nests.

3.10. Co-occurrence matrix sheds light on phenotypic tumor evolution

While snapshots of architectural composition of individual tumors reveal marked complexity, we wondered whether the collection of tumors in (presumably) different stages of evolution could reveal trends in the progression of the compositional landscape over longer timescales. We reasoned that tumors in similar stages of morphological evolution would display similar architectural compositions, and if one architecture did frequently evolve into another, we would find tumors exhibiting both architectures simultaneously. In contrast, we postulated that subtypes that were rarely observed together were unlikely to evolve into each other.

We applied these concepts to the cohort of 549 tumors. We approached the problem mathematically and generated a

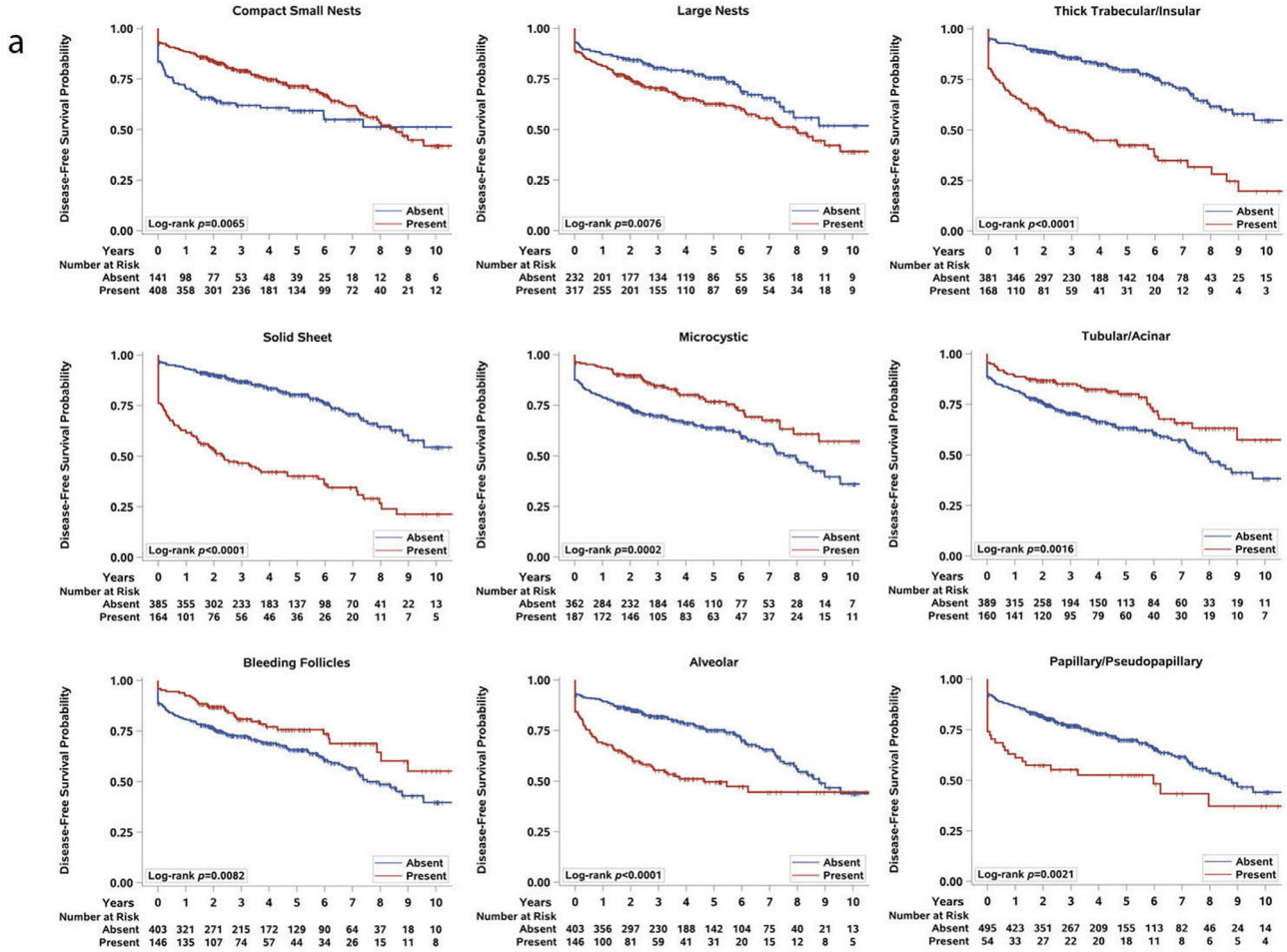

Fig. 3. Analysis of the architectural (a), cytologic and tumor-microenvironment (TME) (b), subtypes and disease-free survival (DFS). Kaplan-Meier plots for DFS and the presence of each architectural, cytologic and TME feature. Log-rank *p*-values are stated. Because our cohort included patients with synchronous metastasis, there was an initial steep decrease in survival.

co-occurrence matrix. We hypothesized that if the evolutionary process was stochastic, no differences would be observed in the frequency with which any two subtypes co-occurred in a tumor. On the other hand, if the process was not stochastic, preferential associations would be observed.

We sought to study how often different patterns co-occurred, and generated a co-occurrence matrix (Fig. 5b). Far from homogeneity, the matrix revealed profound differences in the co-occurrence of different features, with some features rarely observed together in tumors and other features co-occurring at frequencies higher than 80%. These data show that the process whereby different subtypes arise from an ancestral clone is not stochastic. Further, the co-occurrence patterns likely reflect evolutionary constraints.

More specifically, we observed that the majority of solid tumors also had an insular component and large nests as well as compact nests. In contrast, solid tumors infrequently had microcystic, bleeding follicles, or tubular components suggesting mutual exclusivity. Interestingly, we discovered an association between intratumoral lymphocytic infiltrates and sarcomatoid and rhabdoid subtypes.

3.11. t-SNE identifies recurrent evolutionary trajectories converging on solid sheet tumors

Next we sought to build an integrated model going beyond pair-wise co-occurrence matrices. To visualize relationships in more detail, we generated a t-distributed stochastic neighbor embedding (t-SNE) representation of our 549 primary samples based on their architectural composition. Tumors with pure compositions were used as anchors to infer the relationship between architectures. We hypothesized that tumors displaying a single architecture represented either initiating events or terminal events, where a very aggressive subtype may have overtaken the tumor. Where a dominant pattern was the result of a terminal event, tumors may be larger. Of the 73 tumors with a single pattern, 78% ($n = 57$) were comprised solely of compact nests (mean size 4.4 cm), and 5.5% of microcysts (mean size 4.8 cm). Though 8% ($n = 6$) of single pattern tumors were comprised solely of solid, these were significantly larger (mean size 9.5 cm) than those comprised solely of compact nests ($p < 0.0001$) or of microcysts ($p = 0.0085$). These data suggest that compact nests and microcysts are initiating events whereas solid tumors represent a terminal event. Consistent with this notion, whereas compact nests and microcysts were typically of low grade, solid tumors were consistently of high grade. Further, in a subset of tumors, the aggressive architecture seemed to outgrow and almost completely replace the more indolent components, although a small rim of an indolent subtype (often compact nests) could be identified (Supplemental Figure S2b,c).

For most samples that exhibited several architectures, their spatial distribution in the t-SNE plot depended upon the percentage of each pattern. Each sample was color-coded according to the

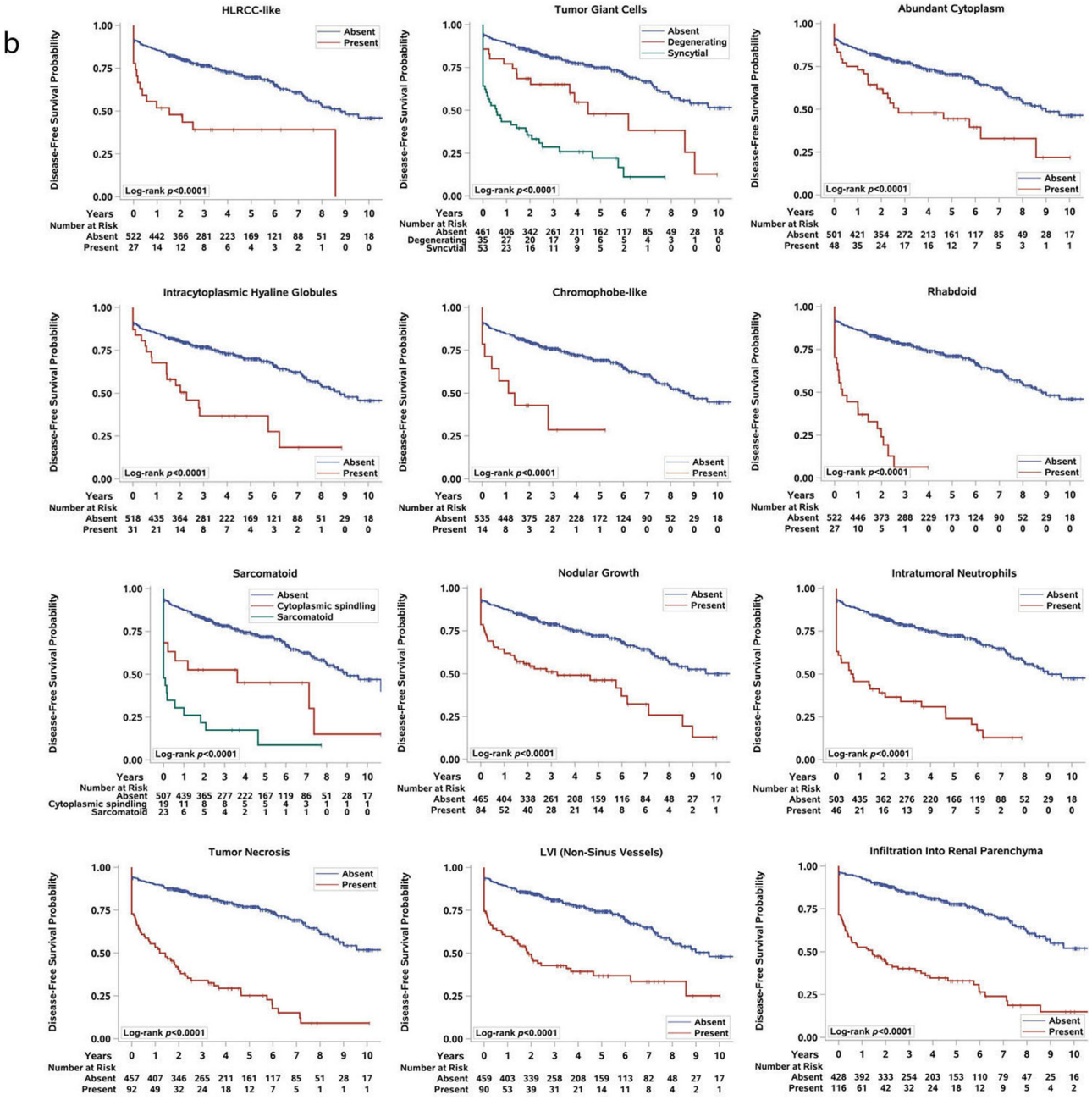

Fig. 3. Continued

dominant architecture (highest percentage in sample composition) (Fig. 6a). As samples of similar dominant architectures clustered together (Fig. 6a and Supplemental Figure S8), the relative locations of the tumors in the t-SNE plot potentially serve as a readout of their evolutionary relationships.

Since tumors evolve from smaller to larger, and from lower to higher grade, we annotated the plots with either tumor size or grade (Fig. 6b-c). Interestingly, both overlays showed a non-random distribution of tumor size and grade with similar convergence for larger, higher grade on solid tumors.

We expanded these analyses by superimposing cytologic and TME features (Supplemental Figure S9). Interestingly, we found that while some features, such as a central scar, were homogeneously distributed across subtypes, others were unequivocally polarized. We were pleased to find that features of advanced tumors, such as infiltration into the renal parenchyma, or into the vasculature (LVI), were enriched in solid tumors. Similarly, cytologic features associated with aggressive evolution such as sarcomatoid or rhabdoid differentiation were also enriched in the solid subtype. Tumor necrosis, which is a poor prognostic factor, was similarly enriched in solid tumors. These findings added credence to our evolutionary model. Perhaps of highest interest, we discovered new associations. In particular, we found a robust association of neutrophilic infiltration with solid tumors.

The rich, non-linear structure of the composition landscape suggests that there may be different evolutionary trajectories that started with compact nests or microcystic subtypes that progressed to a more advanced solid subtype (shown by dotted arrows in Fig. 6a). These data suggest that compact nests progress over time as they grow in size and grade into large nests, insular, and eventually solid subtypes. Similarly, alveolar tumors appear to give rise to large nests and papillary tumors (Fig. 6a). Another interesting

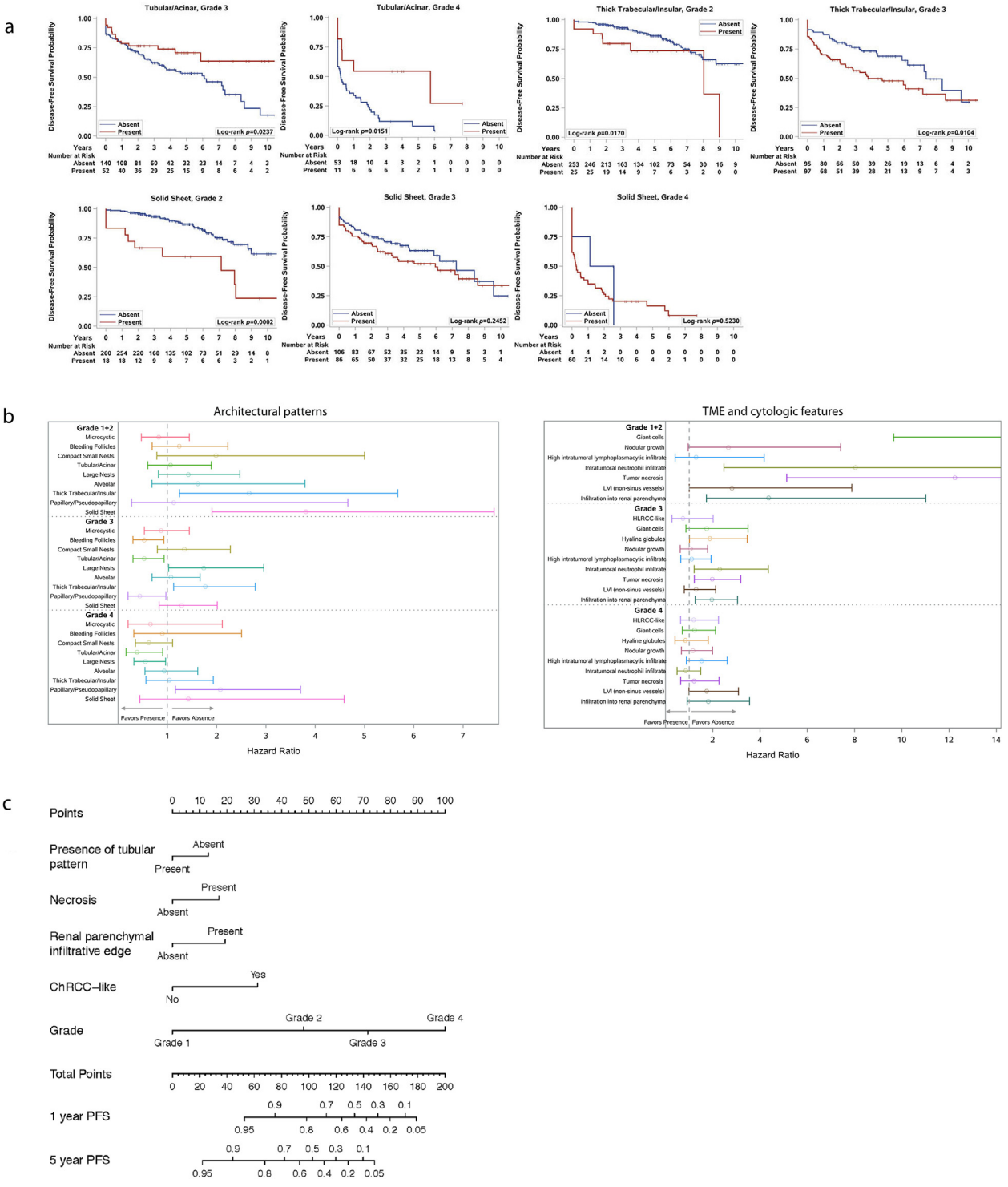

Fig. 4. Integration of phenotypic subtypes and current prognostic variables. (a) Analysis of the architectural features and disease-free survival (DFS) corrected for nucleolar grade. Kaplan-Meier plots for DFS and the presence of architectural patterns in tumors with different nucleolar grades. Log-rank *p* values are stated. **(b) Subgroup analysis of architectural (left), cytologic and TME (right) features and DFS for each grade.** Circles indicate the estimated hazard ratio, and length of the whisker indicates the 95% confidence interval of the estimate. A hazard ratio of greater than 1 indicates that within the given grade, absence of the feature is associated with better DFS as compared to presence of the feature; a hazard ratio of less than 1 indicates that within the given grade, presence of the feature is associated with better DFS as compared to absence of the feature. **(c) Predictive nomogram in ccRCC patients after nephrectomy.**

finding was that the transition from an indolent to an aggressive subtype was accompanied by a reduction in vascularity (Supplemental Figure S7a). These data suggest a coordinated evolutionary process that involves changes not only in architecture, but also vascularity.

3.12. Advanced architectural patterns in the primary tumor seed the development of tumor thrombi

Thrombus formation is a late event in the evolutionary trajectory of ccRCC and it is a common route to metastasis [32]. In addition, inasmuch as tumor extensions into the vasculature

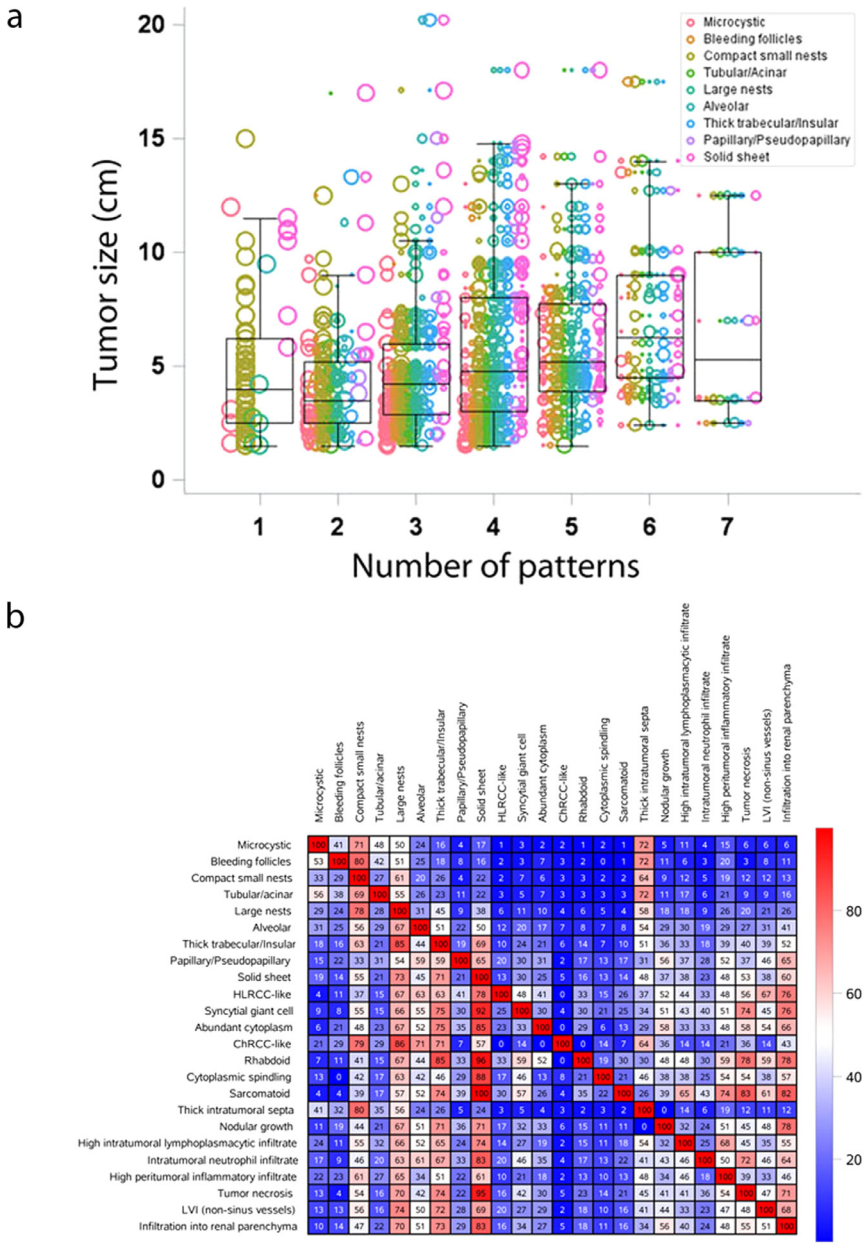

Fig. 5. Intratumoral heterogeneity in ccRCC and co-occurrence of subtypes. (a) Tumor heterogeneity (represented as the number of patterns identified in a tumor) and tumor size. Each sample is represented by multiple dots based on the composition of the patterns it contained, and the size of the dot represents the proportion of the tumor with that pattern. The length of the whiskers are the maximum and minimum observation before 1.5 times the IQR above the 75th percentile or below the 25th percentile, respectively. **(b) Heat map analysis of the morphologic subtypes and conditional positive agreement analysis**. This table is not symmetric; hence, it matters which direction one searches for the same pair. For example, of tumors that developed a large nest pattern, 45% also developed a trabecular/insular pattern; whereas of tumors with a thick trabecular/insular pattern, 85% also developed a large nest pattern.

are constrained - they follow the vessel - they offer an element of directionality that is not otherwise available in tumors, where direction of growth cannot be inferred. Consistent with this notion, we observed that thrombi had limited architectural heterogeneity with a single, typically dominant architecture. To test the directionality hypothesized in our t-SNE plot, we compared the architectural compositions of primary tumors and matched thrombi (Table 2A). As expected, the architectural patterns observed in the thrombi were already present in the matched tumor in the kidney. Interestingly, while most of the architectures observed in kidney tumors were observed in the thrombus, they were observed with a varying incidence, and microcystic and bleeding follicles were never found in the thrombus, even when comprising a significant proportion of the kidney tumor (Fig. 6d, Table 2B). Further, thrombi were enriched for advanced/aggressive architectural patterns even if they represented only a small fraction of the tumor in the kidney. Taken together, these results are supportive of a process whereby more advanced architectural patterns in the kidney tumor seed the development of a thrombus, and provide additional validation for the evolutionary model.

3.13. Tumor reconstitution competency in patient-derived xenograft models provides additional validation of evolutionary trajectories towards aggressive architectural patterns

Metastatic competence is an acquired late event during tumor evolution [13]. The process of metastasis involves invasion into the vasculature, survival in the blood (or lymph stream), extravasation,

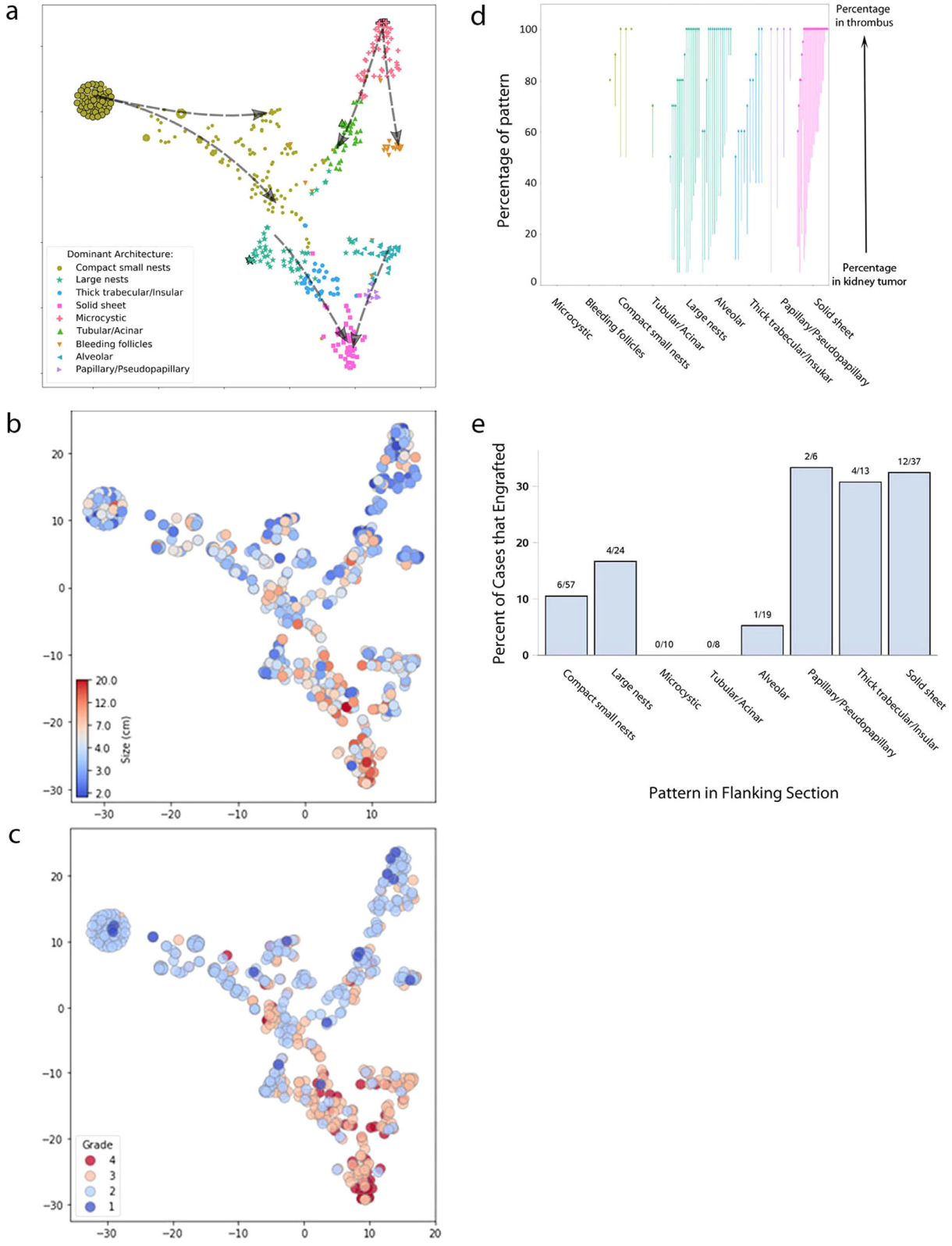

Fig. 6. Morphologic evolutionary trajectories in ccRCC. (a) Architectural evolution model, t-SNE plot based on the architectural composition of each tumor, dashed arrow indicating hypothesized evolution directions with overlaid (b) tumor size, (c) nucleolar grade. Each point on the plot represents a single sample, and the color is based on the dominant pattern present in that tumor. Tumors with a single pattern are indicated with a black border to represent possible truncal patterns. As t-SNE uses relative distances to generate embedding, the axes are essentially arbitrary and are hence not displayed; however, the same scale is used for both axes. The dashed arrow was drawn manually to represent the hypothetical evolutionary trajectory. **(d) Morphologic patterns in thrombus evolution.** Plot showing the percentage of dominant architectural patterns in primary tumors that seeded the tumor thrombus. Each arrow represents an individual ccRCC with a paired thrombus. The tail of the arrow represents the percentage of that architecture in the primary tumor, and the head of the arrow represents the percentage in the paired thrombus. **(e) Comparison of the engraftment rates in mice based on architectural pattern.** Plot showing the percentage of successful stable (lines that could be passaged at least twice in mice) engraftment from 174 ccRCCs implanted in mice and the architectural pattern observed in the flanking H&E stained sections. The odds ratio for engraftment of aggressive patterns as compared to indolent patterns was 3.02 (95% CI 1.31, 6.92; $p = 0.0104$).

Table 2A
Comparison of the presence of architectural patterns in primary and paired thrombi in clear cell renal cell carcinomas with and without a thrombus.

	Thrombus present; Pattern in thrombus Frequency (%) ($n = 82$)	Thrombus absent; Pattern in kidney Frequency (%) ($n = 467$)	p-value
Microcystic	0 (0.0%)	175 (37.5%)	<0.0001
Tubular/Acinar	1 (1.2%)	141 (30.2%)	<0.0001
Bleeding follicles	0 (0.0%)	134 (28.7%)	<0.0001
Compact small nests	13 (15.9%)	362 (77.5%)	<0.0001
Large nests	26 (31.7%)	256 (54.8%)	0.0001
Alveolar	18 (22.0%)	108 (23.1%)	0.8155
Papillary/Pseudopapillary	4 (4.9%)	36 (7.7%)	0.3630
Thick trabecular/Insular	14 (17.1%)	108 (23.1%)	0.2240
Solid sheet	36 (43.9%)	106 (22.7%)	<0.0001

Table 2B
Comparison of the presence of architectural patterns present in primary, and whether or not they are present in thrombus.

	N in thrombus/N in primary (%)	Primary doesn't go to thrombus		Primary goes to thrombus		p-value
		Median% (IQR)	Range	Median% (IQR)	Range	
Microcystic	0/12 (0%)	5 (5–12.5)	5–45	–		–
Tubular/Acinar	1/19 (5.3%)	10 (5–20)	5–60	50		0.1266
Bleeding follicles	0/12 (0%)	7.5 (5–15)	5–30	–		–
Compact small nests	13/46 (28.3%)	15 (10–40)	5–95	60 (50–80)	10–100	0.0005
Large nests	26/61 (42.6%)	15 (10–20)	5–40	30 (10–40)	5–50	0.0171
Alveolar	18/38 (47.4%)	10 (10–22.5)	5–35	30 (10–55)	5–90	0.0247
Papillary/pseudopapillary	4/18 (22.2%)	10 (10–35)	5–50	40 (17.5–65)	5–80	0.2348
Thick trabecular/insular	14/60 (23.3%)	10 (5–20)	5–50	40 (20–40)	10–70	0.0002
Solid sheet	36/58 (62.1%)	15 (5–25)	5–35	50 (20–67.5)	5–100	<0.0001

and reconstitution of the tumor at a distant site. The rate limiting step appears to be the ability of tumor cells to initiate tumorigenesis at a distant site. This is supported by the finding that circulating tumor cell numbers far exceed (by several logs) in most instances the number of appreciable metastatic sites [33]. Currently, there are no assays to test for metastatic competence. However, some literature suggests that metastatic competency may be inferred from tumor growth in a heterologous host [34]. When cells from primary tumors are transplanted into mice, they need to survive, elicit angiogenesis and establish a cooperative relationship with the host stroma in order to grow. In renal cancer, only about 15% of primary tumors are able to form tumors in mice [26]. We have previously shown that samples from metastatic sites engraft at higher frequency than those from primary tumors, and stable engraftment of primary tumors predicts for poor patient survival [26].

We tested the notion of directed evolution towards more aggressive subtypes by leveraging our state-of-the-art tumorgraft (or PDX) platform. Over the years, we have transplanted over 1300 independent patient samples (mostly from primary tumors) into NOD/SCID mice. Among the 549 tumors in this cohort, 149 (174 tumor samples) were transplanted into mice. When tumors are transplanted into mice, samples ~2 mm in diameter are implanted in the kidney, underneath the renal capsule. We correlated the pattern of the sample with stable engraftment in mice (defined by subsequent growth in two serial cohorts of mice with histological validation). We hypothesized that patterns that develop early during the ontological process would fail to engraft compared to more advanced patterns. We found that the frequency of stable engraftment was significantly higher for the aggressive patterns as compared to the indolent patterns (Fig. 6e). The odds ratio for the engraftment of aggressive subtypes as compared to indolent subtypes was 3.02 (95% CI 1.31, 6.92; $p = 0.0104$). Overall, by assaying for the ability to reconstitute tumorigenesis in a different host, we were able to empirically validate the aggressive behavior of the more advanced architectural patterns. Taken together, these data provide strong support for an ontological model of phenotypic tumor evolution converging into a solid subtype.

4. Discussion

In this study, we systematically and comprehensively captured the spectrum of morphologic changes observed in ccRCC. We evaluated the spatial architecture and cytologic features, as well as the TME. We found nine main architectural patterns and twenty-four cytological and TME features. A subset of these features was associated with aggressive biology, significantly worse outcomes, and differential response to targeted therapies. By analyzing patterns of spatial and temporal co-occurrence, we were able to identify distinct trajectories of morphological evolution and found preferential selection for more advanced architectures in vascular extensions and tumors acquiring metastatic competency.

The behavior of a tumor is currently thought to be best predicted by its most aggressive subclone, which forms the basis for assigning tumor grade. Consistent with this notion, the presence of "aggressive" patterns, regardless of their proportion, was associated with a high overall nucleolar grade, aggressive cytologic features, tumor infiltration, and poor outcomes. However, after controlling for nucleolar grade as well as sarcomatoid/ rhabdoid elements in our multivariate analysis, we found that the presence of a tubular component, ChRCC-like pattern, infiltration into the renal parenchyma, and necrosis remained predictive of DFS (Table 1).

Even though genetic evolution and corresponding heterogeneity in a tumor may largely be unpredictable at short timescales, evolutionary constraints lead to the emergence of systematic trends towards metastasis. Accordingly, while the exact morphological changes (which are likely driven by genetic events) in a tumor are unlikely to be predictable, our results suggest broad trends in the evolution of ccRCC architectural composition. The relative locations of the architectures in the t-SNE plot provides a readout of their relationships and reflects evolutionary constraints towards a selection of patterns with aggressive biology. Using the overall change of architectural composition with tumor size/grade vectors, we postulate evolutionary trajectories that start with compact nests or microcysts and progress towards more aggressive architectures. The overlay of the aggressive cytologic and TME features matched with the advanced architectural patterns in the tumor evolution.

Overall, our data are consistent with an evolutionary process that converges on solid tumors.

This model of tumor evolution was also evaluated from the perspective of intravascular tumor extensions, where directionality can be inferred. Thrombi appeared to be more homogeneous than primary tumors and contained only 1–2 different patterns, in contrast to a median of 3.2 patterns for tumors in the kidney, a finding consistent with previous genomic data [13]. We performed comparative analyses of tumor thrombi with the tumors in the kidney and arrived at the following conclusions. First, no pattern was observed solely in the thrombus, rather, when a particular subtype(s) was found in the thrombus, it was also present in the tumor in the kidney. These data suggest that clonal evolution occurred prior to vascular invasion. Second, most patterns were present in the thrombus, except microcystic and bleeding follicles, which may lack invasive potential. Third, we found patterns of low aggressiveness in thrombi suggesting that contrary to what is generally accepted, vascular invasion may be, at least in some instances, an early event. Fourth, we observed an overrepresentation of aggressive patterns in tumor thrombi providing independent validation for the preferential selection for more advanced architectures during the invasive spread from the primary tumor to the thrombus.

We tested the degree of aggressiveness of the different subtypes by analyzing their ability to reconstitute tumor formation in a heterologous host, a process that requires not only survival, but also the ability to establish a cooperative relationship with the host stroma and elicit angiogenesis. We found that the rates of stable tumor engraftment in mice were three times higher for tumors with aggressive components compared to those with indolent subtypes. Overall, these data independently validate the aggressive behavior of a subset of architectural patterns. Given the ability of these evolved tumor cells to reconstitute tumorigenesis in a different host, they may similarly be able to do so at metastatic sites, and accordingly, the presence of such patterns in tumors should raise the concern for metastases, even if not observed at that time.

An interesting set of observations emerged from analyses of the relationship between angiogenesis and tumor evolution. Angiogenesis appears to be central to the development of ccRCC. In fact, the signature genetic event is the loss of *VHL* gene, which results in constitutive activation of HIF and angiogenesis. *VHL* inactivation is not only the most consistent genetic event, but also the only uniformly truncal event. Thus, it would appear that VHL loss is necessary for ccRCC initiation. In fact, the role of *VHL* in tumor formation was confirmed in our tumor studies in mice, were we found that *PBRM1* or *BAP1* loss alone were not sufficient for tumor development [35]. Rather provocatively, given these observations, we found that the vasculature was progressively lost as tumors evolved into more aggressive subtypes. We visualized an evolutionary trajectory of architectural patterns as they lose their dependency or proximity to vasculature, progressing from compact to large nests, and then to insular and finally solid tumors, with the fibrovascular framework becoming ever more widely spaced. This progressive spacing of the vasculature resulted in vascular insufficiency and necrosis, which was almost never observed in compact nests, but was frequent in insular and solid tumors. Hypoxia may be a driver of tumor aggressiveness [36], and these patterns were significantly associated with an increased frequency of metastasis and poor outcomes. Interestingly, in tumors with prominent necrosis, we found that marked pleomorphism, sarcomatoid and rhabdoid morphologies were often observed around areas of necrosis, supporting the notion that hypoxia may be a driver of aggressive phenotypes.

The progressive reduction in vasculature during ccRCC tumor evolution may also have therapeutic implications. Indeed, angiogenesis inhibitors represent the largest class of medications used for the treatment of advanced ccRCC. Inasmuch as these drugs target VEGFR2, which is expressed on endothelial cells, it stands to reason that their activity would be contingent upon the presence of a tumor vascular network. This is supported by recent observations that the expression of genes associated with angiogenesis (such as VEGFA, VEGFR2, and CD31) in tumors predicts for responsiveness to angiogenesis inhibitors [37]. Our evolutionary model suggests, however, that tumors progressively lose this dependency on angiogenesis, and we would speculate that this may result in the acquisition of resistance to this type of drug. Indeed, patients with tumors composed predominantly of patterns characterized by widely spaced out vascular networks (solid, papillary, and insular) had shorter time to progression on VEGF/R2-targeted therapies.

Our evolutionary model likely represents the phenotypic expression of progressive genomic alterations. Indeed, morphology is a useful proxy for underlying genomics. We previously reported a correlation between histomorphologic features and genetic mutations. These studies were aided by the fact that the most commonly mutated genes in ccRCC are two hit tumor suppressor genes, and mutations result in loss of the protein. Accordingly, immunohistochemistry assays can be developed that allow exquisite analyses of the impact of these mutations on cells. We and others have developed such assays for BAP1, PBRM1, and SETD2 [17,38]. For example, BAP1-negative tumor cells tend to be large, with vesicular round nuclei, prominent nucleoli, and characterized by an alveolar pattern [12]. Interestingly, the same was observed in the cystic tumors of *VHL*- and *BAP1*-floxed mice [35,39].

The compact nests resembled normal human renal tubules, and frequently showed PBRM1 loss (data not shown). Second only to *VHL, PBRM1* is a frequent truncal event. These data suggest that this early pattern may be characterized by *PBRM1* loss and few other alterations. Consistent with this notion, this is the same pattern that we found in *VHL/PBRM1*-floxed mouse models [35]. As tumors evolved, they seemed to develop spatially separate "subclones" with different architectural patterns, and the compact nests were subsequently displaced peripherally or overgrown by "more advanced" subtypes. In these tumors, the more advanced patterns continued to show loss of PBRM1, supporting the notion that loss of PBRM1 is a truncal event.

These studies provide a counterpoint to those of the TRACERx consortium. It is interesting that we observed a median of 3.2 patterns per tumor; similarly, Turajlic et al. found the median number of subclones to be 4 per tumor. While we observed that tumors with multiple patterns tended to be associated with better outcomes than those dominated by solid tumors, Turajlic et al. found that clonal diversification was associated with slower growth and attenuated metastasis, and that in contrast, early fixation of multiple driver events led to rapid growth and metastasis [13,14]. We found that tumors with a large number of different patterns had intermediate stage and grade.

One advantage of morphological analyses over genetic analyses is their feasible incorporation into routine clinical care. At present, genomic profiling is not routinely used and does not impact clinical decision-making in everyday practice. Moreover, the low number of patterns renders our atlas a feasible "screen" that can be performed with routine light microscopy. Because the pathologists typically evaluate multiple tumor sections (at least 1 per cm of maximum tumor dimension), our proposed histomorphologic analysis of tumor evolution overcomes the limitations (expense and long turn-around times) of multiregional genomic analyses. In addition, renal tumor biopsies with aggressive patterns may inform decisions regarding surgery and active surveillance. For example, the presence of "aggressive/advanced" patterns in a core biopsy from a renal mass should raise the concern for future growth and metastatic potential in small renal masses considered for ac-

tive surveillance and the possibility of radiologically occult micrometastatic disease in cT1-T3 ccRCC.

Notable limitations of our study include that this represents the analysis of a single institution retrospective cohort, the lack of a validation cohort, and the fact that manual interpretation of morphology is subject to interobserver variability. In addition, this is undoubtedly a simplified view of the individual evolutionary steps occurring in ccRCC. Prospective efforts focusing on genomic correlations with morphologic findings are ongoing. Nonetheless, this is the first comprehensive analysis to explore morphologic heterogeneity in ccRCC and determine its clinical significance. The establishment of comprehensive morphologic ontology could further refine our understanding and stratification in ccRCC. Furthermore, we believe that this work provides a paradigm for deconvoluting tumor complexity that is applicable to other cancer types.

Declaration of Competing Interest

The authors declare the following as competing interests: No potential conflicts of interest were disclosed by the other authors.

CRediT authorship contribution statement

Qi Cai: Data curation, Writing - review & editing. **Alana Christie:** Formal analysis. **Satwik Rajaram:** Formal analysis, Writing - review & editing. **Qinbo Zhou:** Data curation. **Ellen Araj:** Data curation. **Suneetha Chintalapati:** Validation. **Jeffrey Cadeddu:** Resources. **Vitaly Margulis:** Resources. **Ivan Pedrosa:** Resources. **Dinesh Rakheja:** Writing - review & editing. **Renee M. McKay:** Writing - review & editing. **James Brugarolas:** Writing - original draft, Writing - review & editing, Funding acquisition, Methodology, Conceptualization. **Payal Kapur:** Conceptualization, Formal analysis, Supervision, Writing - original draft, Writing - review & editing.

Acknowledgments

We thank the Kidney Cancer Program, the Clinical Data Warehouse team, and the Tumor Registry at Simmons Comprehensive Cancer Center, and in particular the patients whose tissues serve as the basis for this study.

Funding Sources

This work was supported by Cancer Prevention and Research Institute of Texas grant RP180192 (J. Brugarolas) and P50CA196516 (A. Christie, I. Pedrosa, D. Rakheja, R. McKay, J. Brugarolas and P. Kapur) and endowment from Brock Fund for Medical Science Chair in Pathology and Jan and Bob Pickens Distinguished Professorship in Medical Science (P. Kapur)

Supplementary materials

Supplementary material associated with this article can be found, in the online version, at doi:10.1016/j.ebiom.2019.10.052.

References

[1] Gupta M, Blute ML Jr, Su LM, Crispen PL. Delayed intervention of small renal masses on active surveillance. J Kidney Cancer VHL 2017;4(2):24–30.
[2] Uzosike AC, Patel HD, Alam R, Schwen ZR, Gupta M, Gorin MA, et al. Growth kinetics of small renal masses on active surveillance: variability and results from the dissrm registry. J Urol 2018;199(3):641–8.
[3] Zhang Y, Schoenhals J, Christie A, Mohamad O, Wang C, Bowman I, et al. Stereotactic ablative radiation therapy (SAbR) used to defer systemic therapy in oligometastatic renal cell cancer. Int J Radiat Oncol Biol Phys 2019;105(2):367–75.
[4] Janzen NK, Kim HL, Figlin RA, Belldegrun AS. Surveillance after radical or partial nephrectomy for localized renal cell carcinoma and management of recurrent disease. Urol Clin North Am 2003;30(4):843–52.
[5] Grassi P, Doucet L, Giglione P, Grunwald V, Melichar B, Galli L, et al. Clinical impact of pancreatic metastases from renal cell carcinoma: a multicenter retrospective analysis. PLoS ONE 2016;11(4):e0151662.
[6] McKay RR, Kroeger N, Xie W, Lee JL, Knox JJ, Bjarnason GA, et al. Impact of bone and liver metastases on patients with renal cell carcinoma treated with targeted therapy. Eur Urol 2014;65(3):577–84.
[7] Grignon DJ, Che M. Clear cell renal cell carcinoma. Clin Lab Med 2005;25(2):305–16.
[8] Reuter VE, Tickoo SK. Differential diagnosis of renal tumours with clear cell histology. Pathology 2010;42(4):374–83.
[9] Verine J, Colin D, Nheb M, Prapotnich D, Ploussard G, Cathelineau X, et al. Architectural patterns are a relevant morphologic grading system for clear cell renal cell carcinoma prognosis assessment: comparisons with who/isup grade and integrated staging systems. Am J Surg Pathol 2018;42(4):423–41.
[10] Gerlinger M, Horswell S, Larkin J, Rowan AJ, Salm MP, Varela I, et al. Genomic architecture and evolution of clear cell renal cell carcinomas defined by multiregion sequencing. Nat Genet 2014;46(3):225–33.
[11] Gerlinger M, Rowan AJ, Horswell S, Math M, Larkin J, Endesfelder D, et al. Intratumor heterogeneity and branched evolution revealed by multiregion sequencing. N Engl J Med 2012;366(10):883–92.
[12] Pena-Llopis S, Vega-Rubin-de-Celis S, Liao A, Leng N, Pavia-Jimenez A, Wang S, et al. BAP1 loss defines a new class of renal cell carcinoma. Nat Genet 2012;44(7):751–9.
[13] Turajlic S, Xu H, Litchfield K, Rowan A, Chambers T, Lopez JI, et al. Tracking cancer evolution reveals constrained routes to metastases: tRACERx renal. Cell 2018;173(3) 581–94 e12.
[14] Turajlic S, Xu H, Litchfield K, Rowan A, Horswell S, Chambers T, et al. Deterministic evolutionary trajectories influence primary tumor growth: tRACERx renal. Cell 2018;173(3):595–610 e11.
[15] Sankin A, Hakimi AA, Mikkilineni N, Ostrovnaya I, Silk MT, Liang Y, et al. The impact of genetic heterogeneity on biomarker development in kidney cancer assessed by multiregional sampling. Cancer Med 2014;3(6):1485–92.
[16] Cancer Genome Atlas Research N. Comprehensive molecular characterization of clear cell renal cell carcinoma. Nature 2013;499(7456):43–9.
[17] Joseph RW, Kapur P, Serie DJ, Parasramka M, Ho TH, Cheville JC, et al. Clear cell renal cell carcinoma subtypes identified by BAP1 and PBRM1 expression. J Urol 2016;195(1):180–7.
[18] Kapur P, Pena-Llopis S, Christie A, Zhrebker L, Pavia-Jimenez A, Rathmell WK, et al. Effects on survival of BAP1 and PBRM1 mutations in sporadic clear–cell renal-cell carcinoma: a retrospective analysis with independent validation. Lancet Oncol 2013;14(2):159–67.
[19] Kapur P, Christie A, Raman JD, Then MT, Nuhn P, Buchner A, et al. BAP1 immunohistochemistry predicts outcomes in a multi-institutional cohort with clear cell renal cell carcinoma. J Urol 2014;191(3):603–10.
[20] Moch H, Cubilla AL, Humphrey PA, Reuter VE, Ulbright TM. The 2016 who classification of tumours of the urinary system and male genital organs-part A: renal, penile, and testicular tumours. Eur Urol 2016;70(1):93–105.
[21] Trpkov K, Grignon DJ, Bonsib SM, Amin MB, Billis A, Lopez-Beltran A, et al. Handling and staging of renal cell carcinoma: the international society of urological pathology consensus (ISUP) conference recommendations. Am J Surg Pathol 2013;37(10):1505–17.
[22] Chen W, Hill H, Christie A, Kim MS, Holloman E, Pavia-Jimenez A, et al. Targeting renal cell carcinoma with a HIF-2 antagonist. Nature 2016;539(7627):112–17.
[23] Harrell Jr FE. RMS: regression modeling strategies. R package version 5.1-3.1 2019.
[24] Van der Maaten LJP, Hinton GE. Visualizing data using t-SNE. J Mach Learn Res 2008;9:2579–605.
[25] Pavia-Jimenez A, Tcheuyap VT, Brugarolas J. Establishing a human renal cell carcinoma tumorgraft platform for preclinical drug testing. Nat Protoc 2014;9(8):1848–59.
[26] Sivanand S, Pena-Llopis S, Zhao H, Kucejova B, Spence P, Pavia-Jimenez A, et al. A validated tumorgraft model reveals activity of dovitinib against renal cell carcinoma. Sci Transl Med 2012;4(137):137ra75.
[27] Zigeuner R, Hutterer G, Chromecki T, Imamovic A, Kampel-Kettner K, Rehak P, et al. External validation of the mayo clinic stage, size, grade, and necrosis (SSIGN) score for clear-cell renal cell carcinoma in a single European centre applying routine pathology. Eur Urol 2010;57(1):102–9.
[28] Delahunt B, McKenney JK, Lohse CM, Leibovich BC, Thompson RH, Boorjian SA, et al. A novel grading system for clear cell renal cell carcinoma incorporating tumor necrosis. Am J Surg Pathol 2013;37(3):311–22.
[29] Zhang BY, Cheville JC, Thompson RH, Lohse CM, Boorjian SA, Leibovich BC, et al. Impact of rhabdoid differentiation on prognosis for patients with grade 4 renal cell carcinoma. Eur Urol 2015;68(1):5–7.
[30] Dornbusch J, Zacharis A, Meinhardt M, Erdmann K, Wolff I, Froehner M, et al. Analyses of potential predictive markers and survival data for a response to sunitinib in patients with metastatic renal cell carcinoma. PLoS ONE 2013;8(9):e76386.
[31] Jayson GC, Kerbel R, Ellis LM, Harris AL. Antiangiogenic therapy in oncology: current status and future directions. Lancet 2016;388(10043):518–29.
[32] Psutka SP, Leibovich BC. Management of inferior vena cava tumor thrombus in locally advanced renal cell carcinoma. Ther Adv Urol 2015;7(4):216–29.

[33] Nagrath S, Sequist LV, Maheswaran S, Bell DW, Irimia D, Ulkus L, et al. Isolation of rare circulating tumour cells in cancer patients by microchip technology. Nature 2007;450(7173):1235–9.
[34] Quintana E, Piskounova E, Shackleton M, Weinberg D, Eskiocak U, Fullen DR, et al. Human melanoma metastasis in NSG mice correlates with clinical outcome in patients. Sci Transl Med 2012;4(159):159ra49.
[35] Gu YF, Cohn S, Christie A, McKenzie T, Wolff N, Do QN, et al. Modeling renal cell carcinoma in mice: bap1 and pbrm1 inactivation drive tumor grade. Cancer Discov 2017;7(8):900–17.
[36] Rankin EB, Nam JM, Giaccia AJ. Hypoxia: signaling the metastatic cascade. Trends Cancer 2016;2(6):295–304.
[37] McDermott DF, Huseni MA, Atkins MB, Motzer RJ, Rini BI, Escudier B, et al. Clinical activity and molecular correlates of response to atezolizumab alone or in combination with bevacizumab versus sunitinib in renal cell carcinoma. Nat Med 2018;24(6):749–57.
[38] Ho TH, Kapur P, Joseph RW, Serie DJ, Eckel-Passow JE, Tong P, et al. Loss of histone H3 lysine 36 trimethylation is associated with an increased risk of renal cell carcinoma-specific death. Mod Pathol 2016;29(1):34–42.
[39] Wang SS, Gu YF, Wolff N, Stefanius K, Christie A, Dey A, et al. Bap1 is essential for kidney function and cooperates with VHL in renal tumorigenesis. Proc Natl Acad Sci U S A 2014;111(46):16538–43.